Electroosmotic flow and mixing in microchannels with the lattice Boltzmann method

G. H. Tang[a] and Zhuo Li
State Key Laboratory of Multiphase Flow, School of Energy and Power Engineering, Xi'an Jiaotong University, Xi'an 710049, Shaanxi, China

J. K. Wang
School of Aerospace, Tsinghua University, Beijing 100084, China

Y. L. He and W. Q. Tao
School of Energy and Power Engineering, Xi'an Jiaotong University, Xi'an 710049, Shaanxi, China

(Received 24 May 2006; accepted 21 August 2006; published online 10 November 2006)

Understanding the electroosmotic flow in microchannels is of both fundamental and practical significance for the design and optimization of various microfluidic devices to control fluid motion. In this paper, a lattice Boltzmann equation, which recovers the nonlinear Poisson-Boltzmann equation, is used to solve the electric potential distribution in the electrolytes, and another lattice Boltzmann equation, which recovers the Navier-Stokes equation including the external force term, is used to solve the velocity fields. The method is validated by the electric potential distribution in the electrolytes and the pressure driven pulsating flow. Steady-state and pulsating electroosmotic flows in two-dimensional parallel uniform and nonuniform charged microchannels are studied with this lattice Boltzmann method. The simulation results show that the heterogeneous surface potential distribution and the electroosmotic pulsating flow can induce chaotic advection and thus enhance the mixing in microfluidic systems efficiently. © *2006 American Institute of Physics*.
[DOI: 10.1063/1.2369636]

I. INTRODUCTION

Recent developments in microfabrication technologies enabled a variety of miniaturized fluidic systems consisting of microducts, valves, pumps, nozzles, heat exchangers, and various other microscale systems. The microfluidic devices offer many advantages over conventionally sized systems, including size compactness, disposability, increased functionality, reduced sample volumes, shorter analysis times, and decreased manufacturing costs.

The technological demands on microfluidic systems require a better understanding of the microscale fluidic and thermal transport phenomena, which differ much from the macroscale, generally described by the Navier-Stokes equation and energy equation. For microscale gaseous flow the rarefaction due to the mean free path being comparable to the characteristic flow length has significant effect on the flow characteristics.[1] For microscale liquid flow surface effects such as surface roughness, molecular interactions, and electrokinetic effect are very important. In this paper we focus on one of the electrokinetic phenomena, electroosmosis. Electroosmosis is a very promising technology for pumping liquid in microdevices. Bulk liquid in a microchannel can be moved by applying an external electric field along the length of the channel.

Furthermore, as mentioned above, tremendous efforts on miniaturization of devices for microelectrochemical or biomedical system and for microscale combustion and fuel cells applications have been made in recent years. Electroosmotic flow in microfluidic systems is limited to the low Reynolds number regime, and mixing in theses microfluidic systems becomes a problem due to the negligible inertial effects. As a result species mixing in electroosmotic flow systems is inherently diffusion dominated, requiring both a long mixing channel and retention time to attain a homogeneous solution. Moreover, microstirrers with moving components are usually difficult to build or give serious concern for long-term reliability. It is possible to build micromixers by peristaltic motion or by creating a periodic motion in closed cavities.[2]

Generally speaking, the existing methods with no moving parts for enhancing mixing in electroosmotic flow fall into three categories: time-dependent external electric field, nonuniform zeta potential on the surfaces, and rough wall or irregular microchannel.

In the first category, Soderman and Jonsson[3] theoretically studied electroosmosis in planar and cylindrical geometries with both temporal and spatial resolutions by employing pulsed electric fields. Green *et al.*[4] reported experimental results of frequency-dependent electroosmosis on planar microelectrodes by using an ac electric field and they also analyzed the same problem based on linearized double layer theory in Ref. 5. Barragan and Bauza[6] have experimentally studied the influence of an alternating sinusoidally electric field applied on the electroosmotic flow. Scott *et al.*[7] used a theoretical model of electrode polarization to study the strong frequency-dependent ac electroosmotic flow in planar electrode arrays. Oddy *et al.*[8] experimentally studied the micromixing instability in the oscillating electroosmotic flow. Lastochkin *et al.*[9] proposed a microfluidic pump and mixer

[a]Author to whom correspondence should be addressed; electronic mail: ghtang@mail.xjtu.edu.cn

design based on ac Faradaic polarization. Campisi *et al.*[10] analyzed transient and steady-state electroosmosis in rectangular charged microchannels and studied the time-dependent response to sudden ac applied voltage differences in case of finite electric double layer. The Debye-Huckel approximation has been adopted to allow for an algebraic solution of the Poisson-Boltzmann problem in Fourier space.

In the nonuniform zeta potential category, Keely *et al.*[11] theoretically presented the flow profiles in capillaries by varying the zeta potential as a linear function of the length of channel based on the Debye-Huckel theory. Ajdari[12,13] analyzed electroosmosis with nonuniform surface potential and undulated wall and found circulation regions generated by application of oppositely charged surface heterogeneities to the microchannel wall. Stroock *et al.*[14] experimentally studied the electroosmotic flows in microchannels both with the surface charge varying along a direction perpendicular to the electric field used to drive the flow and with the surface charge pattern varying parallel to the field. Measurements of both of these flows agree well with theory in the limit of thin double layers and low zeta potential. Herr *et al.*[15] analytically and experimentally studied the electroosmotic flow in cylindrical capillaries with nonuniform surface potentials. Ren and Li[16] numerically simulated electroosmotic flow in heterogeneous cylindrical microchannel with nonuniform zeta potential by using momentum equation and linearized Poisson-Boltzmann equation. Erickson and Li[17] studied homogeneous and heterogeneous surfaces as a method of enhancing mixing in T-shaped mixers through three-dimensional (3D) finite-element based numerical simulations. Qian and Bau[18] theoretically investigated two-dimensional, time-independent, and time-dependent electroosmotic flows driven by a uniform electric field in a conduit with nonuniform zeta potential distributions along its walls. Fu *et al.*[19] found that a step change in zeta potential causes a significant variation in the velocity profile and in the pressure distribution by numerically solving the Navier-Stokes equation and the Nernst-Planck equation. Tian *et al.* used the linearized Poisson-Boltzmann equation[20] and nonlinear Poisson-Boltzmann equation[21] to model the electrical double layer and the lattice Boltzmann method coupled with the constraint of current continuity to simulate the microfluidic flow field in a rectangular microchannel with nonuniform surface potentials.

With regard to the third category, rough wall or grooved surfaces, serpentine microchannel, T-shape channel, and so on are investigated, and one can see Refs. [12,13,22–26] for details.

The recent development of the lattice Boltzmann method (LBM) has provided an alternative simulation tool for computational fluid dynamics.[27] As a derivative of lattice gas automata (LGA), the LBM is different from the conventional numerical methods which solve the usual macroscopic governing equations for the conserved fields. The LBM tries to model the fluid flow by tracking the evolution of the distribution functions of the microscopic fluid particles. That means the LBM provides a method to obtain streaming patterns for complicated systems, which is usually difficult for Navier-Stokes equation-based methods. Recently the LBM has also found success in applications to microfluidics. One can see Refs. 28–34 for rarefied gaseous flow in microfluidic systems. Particularly, some efforts have been made to apply the LBM to electrokinetic systems.[20,21,35–38] But most of the studies employed a linearized Poisson-Boltzmann equation[20,38] or solved the nonlinear Poisson-Boltzmann equation[21] with other numerical methods to obtain the electric potential distribution in the liquid, then used a lattice Boltzmann equation to solve the velocity fields, or the used lattice Boltzmann methods to solve the Poisson-Boltzmann equation have some limitations. Guo *et al.*[39] give a summary for the previous LBM studies on the electrokinetic flow and proposed a finite-difference-based lattice Boltzmann algorithm.

Motivated by the growing interest in electroosmosis as a reliable no moving parts strategy to pump liquid, to mix liquid, and to control fluid motion in microfluidic devices, we study steady-state and pulsating electroosmotic flow in two-dimensional parallel uniform and nonuniform charged microchannels using the lattice Boltzmann method. In the present work, we used a lattice Boltzmann equation for the nonlinear Poisson-Boltzmann equation to obtain the electric potential distribution and another lattice Boltzmann equation to solve the velocity fields. The benefit of the present approach is the easiness of programming, since the computations of the electric potential field and the velocity field are in the same framework of the LBM and have the same structures. Especially this feature could be more useful for a multiprocessor code in parallel computing applications. Furthermore, we demonstrate their direct applicability to modeling steady-state and pulsating electroosmotic flow in uniform and nonuniform charged microchannels.

The rest of the paper is organized as follows. In Sec. II, we present the discrete Boltzmann equation for the velocity fields and the electric potential. In Sec. III, two numerical tests are conducted to validate the LBM model. Section IV presents numerical simulations of electroosmotic flow and electroosmotic pulsating flow in homogeneous and heterogeneous charged microchannels. A conclusion is given in Sec. V.

II. LATTICE BOLTZMANN EQUATION

A. The lattice Boltzmann equation for velocity fields

The lattice Boltzmann method simulates transport phenomena by tracking the movements of molecule ensembles through the evolution of the distribution function. The lattice Boltzmann equation can be derived from the Boltzmann equation.[40] The dimensionless Boltzmann-BGK equation with an external force term $\mathbf{F}$ can be written as[41]

$$\frac{\partial f}{\partial t} + \boldsymbol{\xi} \cdot \nabla f + \mathbf{F} \cdot \nabla_{\xi} f = -\frac{f - f^{\mathrm{eq}}}{\lambda}, \tag{1}$$

where $f \equiv f(\mathbf{r}, \boldsymbol{\xi}, t)$ is the single-particle distribution function in the phase space $(\mathbf{r}, \boldsymbol{\xi})$, $\boldsymbol{\xi}$ is the microscopic velocity, $\mathbf{r}$ is the space, $\mathbf{F}$ is the external body force which can depend on both space $\mathbf{r}$ and time t, λ is the relaxation time due to collision, and f^{eq} is the Maxwell-Boltzmann equilibrium distribution,[40]

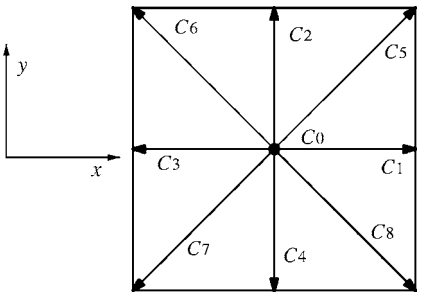

FIG. 1. Schematic of D2Q9 lattice.

$$f^{\mathrm{eq}} = \frac{\rho}{(2\pi RT)^{D/2}} \exp\left[-\frac{(\boldsymbol{\xi}-\mathbf{u})^2}{2RT} \right], \tag{2}$$

where ρ, $\mathbf{u}$, and T are the macroscopic density, velocity, and the temperature, respectively, D is the dimension of the space, and R is the gas constant. It has been shown that the following lattice Boltzmann evolution equation can be derived from the Boltzmann equation, Eq. (1),[42]

$$\frac{\partial f}{\partial t} + \boldsymbol{\xi}\cdot\nabla f = -\frac{f-f^{\mathrm{eq}}}{\lambda} + \frac{\mathbf{F}\cdot(\boldsymbol{\xi}-\mathbf{u})}{RT} f^{\mathrm{eq}}, \tag{3}$$

with $\mathbf{F}$ being the external force acting per unit mass. The second-order Chapman-Enskog approximation of the Boltzmann equation, Eq. (3), recovers the following momentum equations at the Navier-Stokes level:

$$\rho\left[\frac{\partial \mathbf{u}}{\partial t} + (\mathbf{u}\cdot\nabla)\mathbf{u} \right] = \rho\nu\nabla^2\mathbf{u} + \rho\mathbf{F}, \tag{4}$$

with

$$\rho\mathbf{F} = -\nabla p + \mathbf{F}_{\mathrm{ext}} + \rho_e(\mathbf{E}_{\mathrm{int}} + \boldsymbol{\xi}\times\mathbf{B}_{\mathrm{int}}) + \mathbf{F}_{\mathbf{V}}, \tag{5}$$

where ν represents the kinetic viscosity; p represents the externally applied pressure; $\mathbf{F}_{\mathrm{ext}}$ represents the external forces, including the Lorentz force associated with any externally applied electric and magnetic field; ρ_e represents the net charge density per unit volume at any point in the liquid; $\mathbf{E}_{\mathrm{int}}$ and $\mathbf{B}_{\mathrm{int}}$ are internally smoothed electric and magnetic fields due to the motion of all charged particles inside the fluid, respectively; and $\mathbf{F}_{\mathbf{V}}$ is a single equivalent force density due to the intermolecular attraction. For only an electric field, we have $\mathbf{F}_{\mathrm{ext}}=\rho_e\mathbf{E}_{\mathrm{ext}}$, where $\mathbf{E}_{\mathrm{ext}}$ is the external electric field intensity.

The discrete lattice Boltzmann equation with the BGK collision approximation including an external force term can be written as

$$f_i(\mathbf{r}+\mathbf{c}_i\delta_t, t+\delta_t) = f_i(\mathbf{r},t) - \frac{1}{\tau_v}[f_i(\mathbf{r},t) - f_i^{\mathrm{eq}}(\mathbf{r},t)] + \delta_t \frac{\mathbf{F}\cdot(\mathbf{c}_i-\mathbf{u})}{RT} f_i^{\mathrm{eq}}(\mathbf{r},t), \tag{6}$$

where $\tau_v=\lambda/\delta_t$ is the nondimensional relaxation time. The parameter $\mathbf{c}_i$ is the particle discrete velocity. For a square lattice D2Q9 model as shown in Fig. 1, $\mathbf{c}_0=0$ corresponds to the distribution with zero velocity, $\mathbf{c}_i=\{\cos[(i-1)\pi/2], \sin[(i-1)\pi/2]\}c$ for $i=1,2,3,4$ and $\mathbf{c}_i=\{\cos[(i-5)\pi/2+\pi/4], \sin[(i-5)\pi/2+\pi/4]\}c$ for $i=5,6,7,8$, where $c=\delta_x/\delta_t$ is the particle streaming speed and δ_x and δ_t are the lattice spacing and step size in time, respectively.

In Eq. (6) $f_i^{\mathrm{eq}}(i=0,1,\ldots,8)$ stands for the equilibrium density distribution function and for the D2Q9 lattice, one obtains the following form:[42]

$$f_i^{\mathrm{eq}} = \rho\omega_i\left[1 + \frac{3(\mathbf{c}_i\cdot\mathbf{u})}{c^2} + \frac{9(\mathbf{c}_i\cdot\mathbf{u})^2}{2c^4} - \frac{3(\mathbf{u}\cdot\mathbf{u})}{2c^2} \right], \tag{7}$$

where $\omega_0=4/9$, $\omega_i=1/9$ for $i=1,2,3,4$ and $\omega_i=1/36$ for $i=5,6,7,8$. The macroscopic variables such as mass density and the momentum density are defined by sums over the distribution functions $f_i(\mathbf{r},t)$,

$$\rho = \sum_i f_i, \quad \rho\mathbf{u} = \sum_i f_i\mathbf{c}_i. \tag{8}$$

The kinetic viscosity is

$$\nu = \frac{(2\tau_v-1)}{6}\frac{\delta_x^2}{\delta_t}, \tag{9}$$

and the speed of sound is

$$c_S = \frac{1}{\sqrt{3}}c. \tag{10}$$

For electrokinetic flows in dilute electrolyte solutions, the external force term in Eq. (5) can be simplified to

$$\rho\mathbf{F} = -\nabla p + \rho_e\mathbf{E}_{\mathrm{ext}} - \rho_e\nabla\Phi, \tag{11}$$

where Φ is the stream electric potential caused by the ion movements in the solution based on the Nernst-Planck theory. Generally, the stream potential maybe dominate the electroviscosity effect in pressure driven flow, but its value is much less than the external potential and can be neglected in pure electrical driven flows.

B. The lattice Boltzmann equation for electric potential

According to the theory of electrostatics, the relationship between the electric potential in the liquid, ψ, and the net charge density per unit volume, ρ_e, at any point in the liquid is described by the following Poisson equation:

$$\nabla^2\psi = -\frac{\rho_e}{\varepsilon\varepsilon_0}, \tag{12}$$

where ε is the relative dielectric constant of the solution and ε_0 is the permittivity of a vacuum. Assuming that the equilibrium Boltzmann distribution is applicable, the net charge density distribution can be expressed as the sum of all the ions in the solution,

$$\rho_e = \sum_i z_i e n_{i,\infty} \exp\left(-\frac{z_i e\psi}{k_B T} \right), \tag{13}$$

where $n_{i,\infty}$ and z_i are the bulk ionic concentration and the valence of type i ions, respectively. The bulk ionic concentration n_∞ can be expressed as the product of the ionic molar concentration of c_∞ with the Avogadro's number of N_0. Constant e is the charge of a proton, k_B is the Boltzmann constant, and T is the absolute temperature. Substituting Eq. (13)

into Eq. (12) yields the nonlinear Poisson-Boltzmann equation,

$$\nabla^2\psi + \frac{1}{\varepsilon\varepsilon_0}\sum_i z_i e n_{i,\infty} \exp\left(-\frac{z_i e\psi}{k_B T}\right) = 0. \tag{14}$$

Comparing the above equation with the special case of the steady-state laminar incompressible energy equation when the velocity is zero and the thermal diffusivity is unity, we can derive the following discrete lattice Boltzmann evolution equation for the electric potential similar to the treatment of the energy equation in Ref. 43:

$$g_i(\mathbf{r}+\mathbf{c}_i\delta_{t,g}, t+\delta_{t,g}) = g_i(\mathbf{r},t) - \frac{\delta_{t,g}}{\tau_g + 0.5\delta_{t,g}}[g_i(\mathbf{r},t) - g_i^{\mathrm{eq}}(\mathbf{r},t)] + \left(\frac{\tau_g}{\tau_g + 0.5\delta_{t,g}}\right) \times \left[\frac{1}{\varepsilon\varepsilon_0}\sum_i z_i e n_{i,\infty} \exp\left(-\frac{z_i e\psi}{k_B T}\right)\right]\delta_{t,g}\omega_i. \tag{15}$$

The corresponding equilibrium distribution of g^{eq} on the D2Q9 discrete lattice, similar to the energy density equilibrium distribution in Ref. 43, takes the form

$$g_0^{\mathrm{eq}} = 0,$$

$$g_{1,2,3,4}^{\mathrm{eq}} = \frac{\psi}{9} \times \frac{3}{2} = \frac{\psi}{6}, \tag{16}$$

$$g_{5,6,7,8}^{\mathrm{eq}} = \frac{\psi}{36} \times 3 = \frac{\psi}{12}.$$

Corresponding to the thermal diffusivity in the energy equation, the potential diffusivity χ, which is equal to unity in the simulations, can be defined as

$$\chi = \frac{2\tau_g}{3}\frac{\delta_x^2}{\delta_{t,g}}. \tag{17}$$

The macroscopic electric potential in the liquid is calculated as

$$\psi = \sum_i g_i + \frac{\delta_{t,g}}{2}\sum_i \left[\frac{1}{\varepsilon\varepsilon_0}\sum_i z_i e n_{i,\infty} \exp\left(-\frac{z_i e\psi}{k_B T}\right)\right]\omega_i. \tag{18}$$

The present LBM method is relatively simple and can be straightly extended to three-dimensional problems by using D3Q15 (Ref. 42) or D3Q19 lattice model,[44] and, in particular, it is of good numerical stability and of flexibility to deal with complex geometries, since general boundary conditions are easily implemented without special attention.

If assuming uniform dielectric constant and neglecting the fluctuation of the dielectric constant, in other words, the ion-convection effects will be relatively smaller than the ion diffusion effects and can be neglected when the Peclet number is smaller than 100,[45] the net charge density distribution is proportional to the concentration difference between the cations and anions,

$$n_{\pm} = n_\infty \exp\left(\mp\frac{ze\psi}{k_B T}\right), \tag{19}$$

$$\rho_e = ze(n_+ - n_-) = -2zen_\infty \sinh\left(\frac{ze\psi}{k_B T}\right), \tag{20}$$

and thus it yields the following nonlinear Poisson-Boltzmann equation for the electrical potential in the dilute electrolyte solution:

$$\nabla^2\psi = \frac{2zen_\infty \sinh(ze\psi/k_B T)}{\varepsilon\varepsilon_0}. \tag{21}$$

Furthermore, if $ze\psi/k_B T$ is small, the term in Eq. (21) can be assumed as $\sinh(ze\psi/k_B T) \approx ze\psi/k_B T$; equation (21) recovers the following linearized Poisson-Boltzmann equation:

$$\nabla^2\psi = \frac{2n_\infty e^2 z^2 \psi}{\varepsilon\varepsilon_0 k_B T} = \frac{\psi}{\lambda_D^2}. \tag{22}$$

The linearized simplification of Eq. (22) was solved or employed in Refs. [5,10–13,16,46–48]. The Debye length λ_D, a measure of the distance over which an individual charged particle can exert an effect, is calculated by

$$\lambda_D = \sqrt{\frac{\varepsilon\varepsilon_0 k_B T}{2n_\infty e^2 z^2}}. \tag{23}$$

C. The boundary condition for the lattice Boltzmann equation

Attention is now turned to the boundary conditions. In the LBM and the LGA, the so-called nonslip boundary condition, namely, zero fluid velocity at a given solid surface, is obtained usually with bounce-back refection. The easy implementation of this nonslip velocity condition by the bounce-back scheme supports the idea that the LBM is ideal for simulating fluid flows in complex geometries. However, it has been confirmed that the bounce-back scheme is only of first order in numerical accuracy at the boundaries,[49] which degrades the LBM, because numerical accuracy of the LBM is of second order in the interior points. To overcome this shortage, many improvements have been proposed. Ziegler[50] shifted the boundary into the fluid by half mesh unit and then used the bounce-back scheme. Inamuro *et al.*[51] introduced a nonslip boundary condition in which a counter slip velocity was used to cancel the effect of a slip velocity induced by the bounce-back scheme near wall nodes. Zou and He[52] extended the bounce-back condition for the nonequilibrium portion of the distribution function. Chen *et al.*[53] proposed a second-order extrapolation scheme of distributions in the flow to obtain the unknown particle distributions. D'Orazio *et al.*[54] assumed a counter slip thermal energy density which is determined consistently with Dirichlet or Neumann boundary constraints. Tang *et al.*[55] used a first-order extrapolation to deal with the Dirichlet or Neumann boundary in the doubled populations thermal LBM. Here we adopted the nonslip boundary conditions by Zou and He[52] on the upper and bottom walls to solve the density distribution function for velocity fields. With regard to the lattice Boltzmann equation for the electric potential, the zeta potentials on the upper and bottom walls are known in the simulation and we employed the Dirichlet boundary condition in our previous

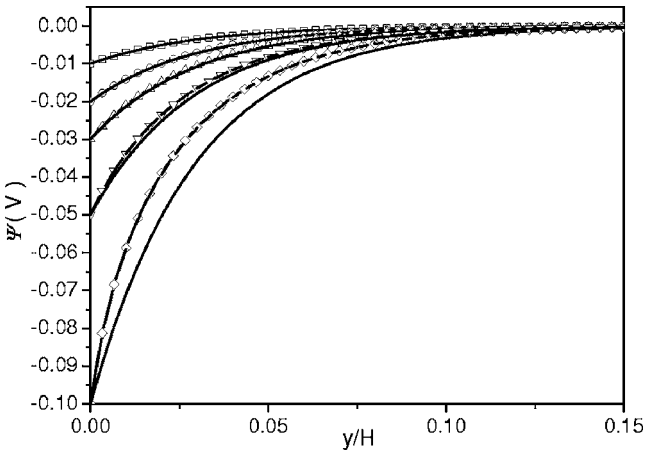

FIG. 2. The electric potential comparisons of the LBM results (open symbols), the solutions of the linearized Poisson-Boltzmann equation (solid lines), and the numerical results of the nonlinear Poisson-Boltzmann equation with the finite volume method (dashed lines).

work.[55] For the channel inlet and the outlet, we employed periodic boundary conditions by assuming a fully developed flow.

III. VALIDATION OF THE MODEL

A. The electroosmotic potential distribution in the liquid

The simple geometry of an electrolyte confined between two parallel plates is considered. The lower and upper surfaces are defined by $y=0$ and $y=H$. Unless otherwise mentioned, in this paper, the simulated channel height is $H=1$ μm, $\varepsilon\varepsilon_0=6.95\times10^{-10}$ C^2/J m, $T=273$ K, $e=1.6\times10^{-19}$ C, $z=1$, $N_0=6.02\times10^{23}$, $k_B=1.38\times10^{-23}$, $\rho=1000$ kg/m^3, and $\nu=1.789\times10^{-5}$ m^2/s. Figure 2 shows the electric potential distribution across the channel. The open symbols in the figure represent the LBM results for the nonlinear Poisson-Boltzmann equation, the solid lines represent the analytical solutions of the linearized equation, and the dashed lines represent the results by numerically solving the nonlinear Poisson-Boltzmann equation with the finite volume method using our own developed code. The electric potential in the liquid between the channels is decreasing from a given zeta potential (commonly assumed to be equal to the electrostatic surface potential) ζ to zero at middle of the channel height. We can see that the present LBM results agree with the linearized analytical solutions very well when the zeta potential is very small; however, the discrepancy increases as the zeta potential increases, which implies that the linearization of the Poisson-Boltzmann equation is limited to small zeta potential, usually, say, less than 25 mV.[46] The LBM solutions are in good agreement with the macroscale numerical results of finite volume method for all the cases.

B. Pressure driven pulsating flow

Consider the two-dimensional Womersley flow in a plane channel. The flow is driven by a periodic pressure gradient given by

$$\frac{\partial p}{\partial x} = \mathrm{Re}[Ae^{i\omega t}], \tag{24}$$

with an amplitude $A=\Delta p/\Delta x$ and a frequency ω. The linear pressure distribution of the developed flow in the streamwise direction is assumed and thus the value A is a constant. The solution of the Navier-Stokes equation assuming a laminar flow can be found in Ref. 56.

In the LBM simulation, the pressure gradient $\Delta p/\Delta x$ is fixed at -10^6 Pa/m and the time step $\delta_t=2.5\times10^{-12}$ s. T_p represents the period of the pulsating driving pressure normalized by δ_t, $\omega=2\pi/(T_p\delta_t)$, and α represents the Womersley number, $\alpha=H\sqrt{\omega/\nu/2}$.

Figure 3 shows the streamwise velocity profiles normalized by $u_{\max}=(H^2/8\mu)(\Delta p/\Delta x)$ at eight different times. When the period is short the velocity profiles are quite complicated, annular effects exist in the velocity profiles, and the velocity near the wall may be larger than the velocity at the centerline at some moments, which can enhance the flow mixing effect near the wall. However, the velocity profiles are of parabolic type when the period is longer, and the velocity at the centerline is always larger than the velocity near the wall at any moment. The solid lines represent the analytical solutions, and the symbols represent the LBM results. We can also see that the agreement is excellent. From the above two tests, we can believe that the present LBM model is valid.

IV. RESULTS AND DISCUSSION

A. Electroosmotic flow in homogeneous microchannels

A uniform external electric field E is applied parallel to the plane channel, and the lower and upper surfaces are distributed with uniform zeta potential. Figures 4(a) and 4(b) show the streamwise velocity profiles across a section of the channel at the middle (in Fig. 4, the units of E and ζ are V/m and mV, respectively). The Debye length calculated with Eq. (23) in Fig. 4(a) is 0.029 15 μm, much lower than the channel height, 1 μm. Comparing the four cases shown in the figure, we can see that as the zeta potential increases or as the external electric field intensity increases, the velocity in the electroosmotic flow nearly increases proportionally. However, for the case shown in Fig. 4(b) with the Debye length 0.9219 μm, which is comparable to the channel height, 1 μm, we can see that the maximum velocity in the electroosmotic flow still nearly increases proportionally as the external electric field intensity increases while the maximum velocity increases more rapidly as the zeta potential increases.

In Fig. 5, the zeta potential on the upper and bottom walls keeps at $\zeta=-50$ mV and the external electric field intensity parallel to the plane channel keeps at $E=500$ V/m. From the bottom to the upper, the bulk ionic molar concentrations are $c_\infty=10^{-8}$, 10^{-7}, 10^{-6}, 10^{-5}, 10^{-4}, and 10^{-3} mol/l and the corresponding Debye lengths are 2.915, 0.9219, 0.2915, 0.092 19, 0.029 15, and 0.009 219 μm. Namely, as the bulk ionic concentration increases, the Debye length decreases. From the figure we can see that as the bulk ionic

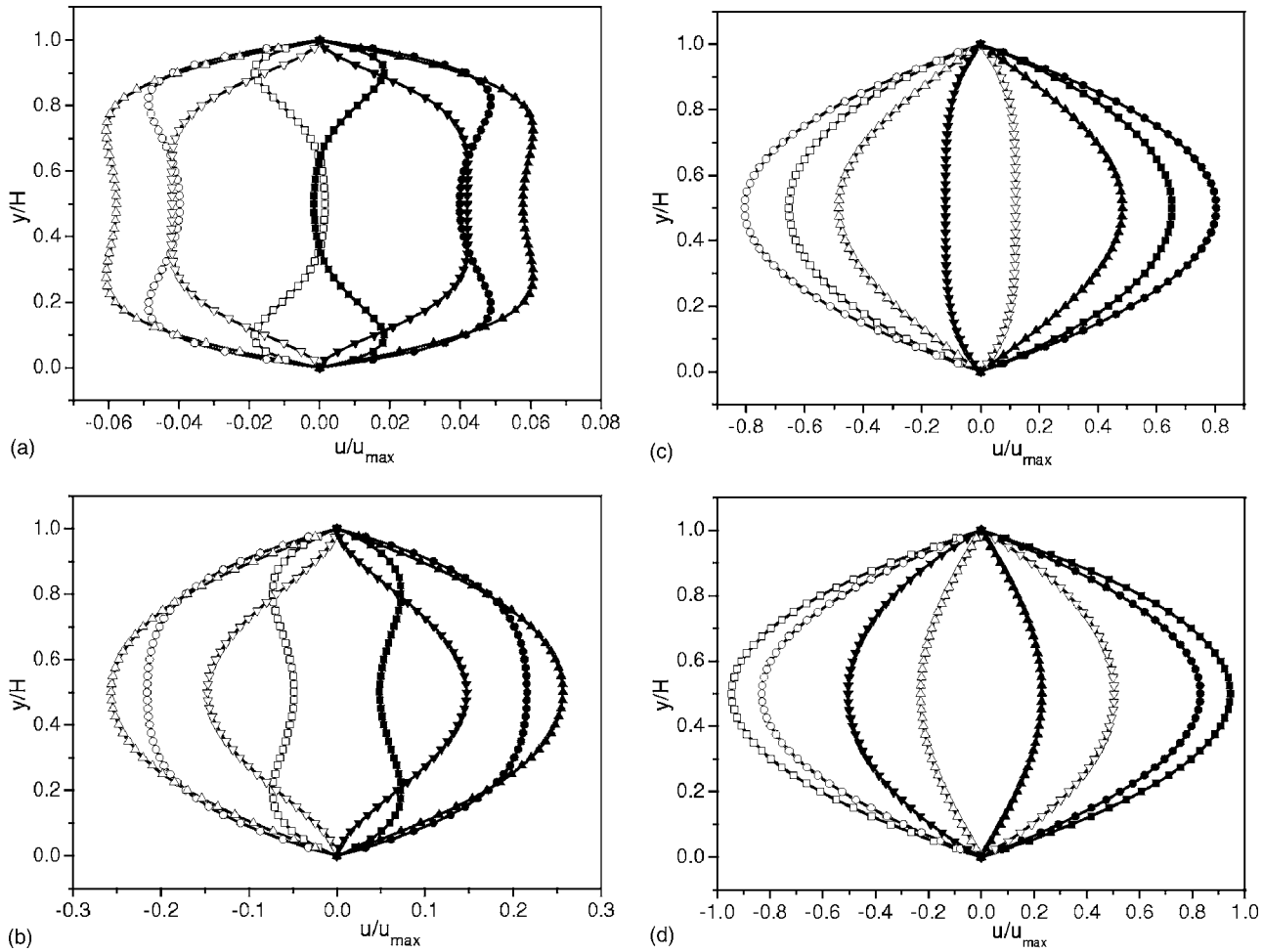

FIG. 3. Normalized velocity profiles of the Womersley flow. The open squares, circles, triangles, and inverted triangles represent the results at $t=0$, $T_p/8$, $T_p/4$, $3T_p/8$, respectively; the closed squares, circles, triangles, and inverted triangles represent the results at $t=T_p/2$, $5T_p/8$, $3T_p/4$, and $7T_p/8$, respectively; and the solid lines represent the analytical solutions. (a) $T_p=10\,000$, $\alpha\approx 5.93$. (b) $T_p=40\,000$, $\alpha\approx 2.96$. (c) $T_p=200\,000$, $\alpha\approx 1.33$. (d) $T_p=600\,000$, $\alpha\approx 0.76$.

concentration increases, the velocity profiles across the channel develop sharp features in the near vicinity of the wall. We can also see that the velocity increases sharply very near the wall and then keeps a constant nearly in the most of channel region when the Debye length is much lower than the channel height. But the velocity profiles across the channel present to be obvious parabolas as the magnitude of the Debye length increases. More specifically, we can see that the maximum velocity nearly keeps a constant for the shown bulk ionic concentration range of $c_\infty=10^{-3}-10^{-5}$ mol/l when the ratio of the channel height to the Debye length is larger than about 10.

Figure 6 presents the channel height effect on the velocity. From Figs. 6(a) and 6(b) we also find that the velocity distributions in the channel centerline region and the maximum velocity nearly keep a constant when the ratio of the channel height to the Debye length is larger than about 10 [$H\geqslant 3.0$ μm in Fig. 6(a) and $H\geqslant 0.4$ μm in Fig. 6(b)]. We think that the phenomena are caused by the overlapping or closely overlapping of the electric double layers, since the Debye length measures the range of electrostatic influence of the single ions.

B. Electroosmotic pulsating flow in homogeneous microchannels

We study the fluid flow in microchannel geometries by changing the polarity of the externally imposed electric field. Similar to experimental work in Ref. 4, we used very high frequency electric fields to drive the flow. The time periodic external electric intensity is

$$E=\mathrm{Re}[E_0 e^{i\omega t}], \tag{25}$$

with an amplitude E_0 and a frequency ω. In the simulations, the time step is $\delta_t=2.5\times 10^{-12}$ s. T_E represents the period of the externally imposed electric field normalized by δ_t and the external frequency $\omega=2\pi/(T_E\delta_t)$. The bulk ionic concentration is $c_\infty=10^{-4}$ mol/l and the corresponding Debye length is 0.029 15 μm.

Comparing Figs. 7(b) and 7(a), we can see that as the external electric field intensity increases, the magnitude of the velocity increases proportionally. Similar to the pressure driven pulsating flow, when the period is short the velocity profiles are quite complicated; strong annular effects occur in

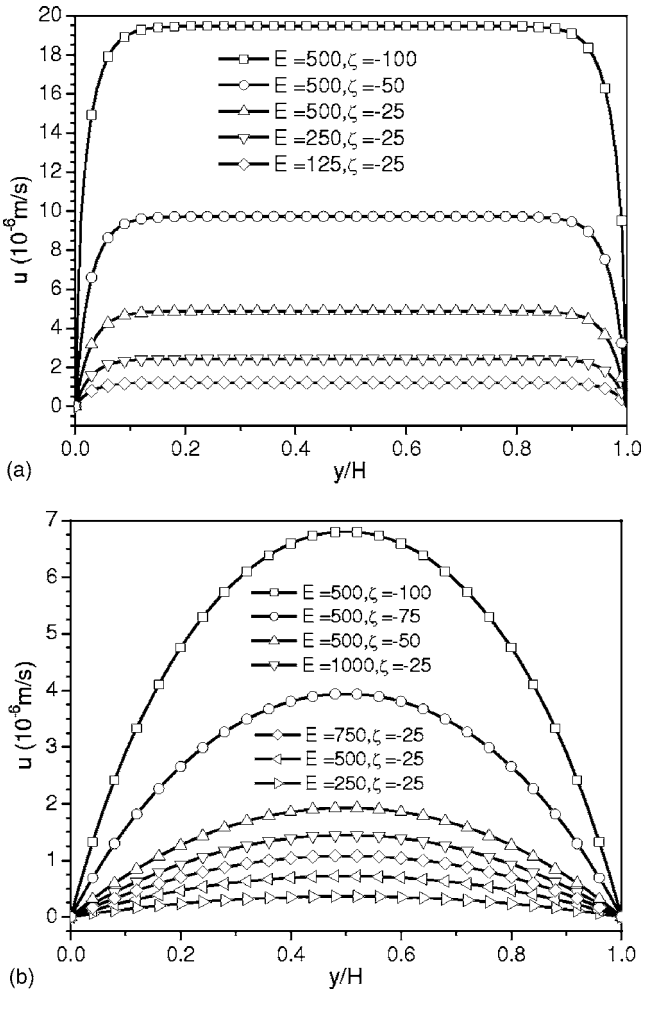

FIG. 4. The streamwise velocity profiles at various external electric field intensities and zeta potentials. (a) $c_\infty = 10^{-4}$ mol/l. (b) $c_\infty = 10^{-7}$ mol/l.

the velocity profiles. As the frequency decreases, the annular effect weakens gradually in the channel. The results show that the time periodic electroosmotic forces act on the fluid as a pulse and can promote mixing effectively.

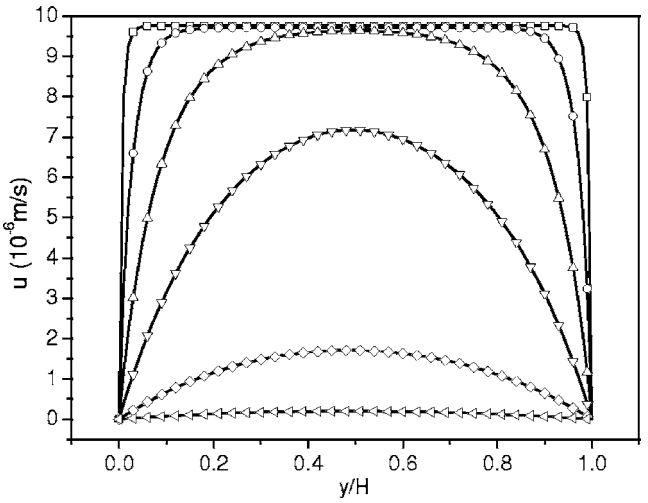

FIG. 5. The streamwise velocity profiles at various bulk ionic molar concentrations. From the bottom to the upper, the bulk ionic molar concentration is $c_\infty = 10^{-8}$, 10^{-7}, 10^{-6}, 10^{-5}, 10^{-4}, and 10^{-3} mol/l, respectively.

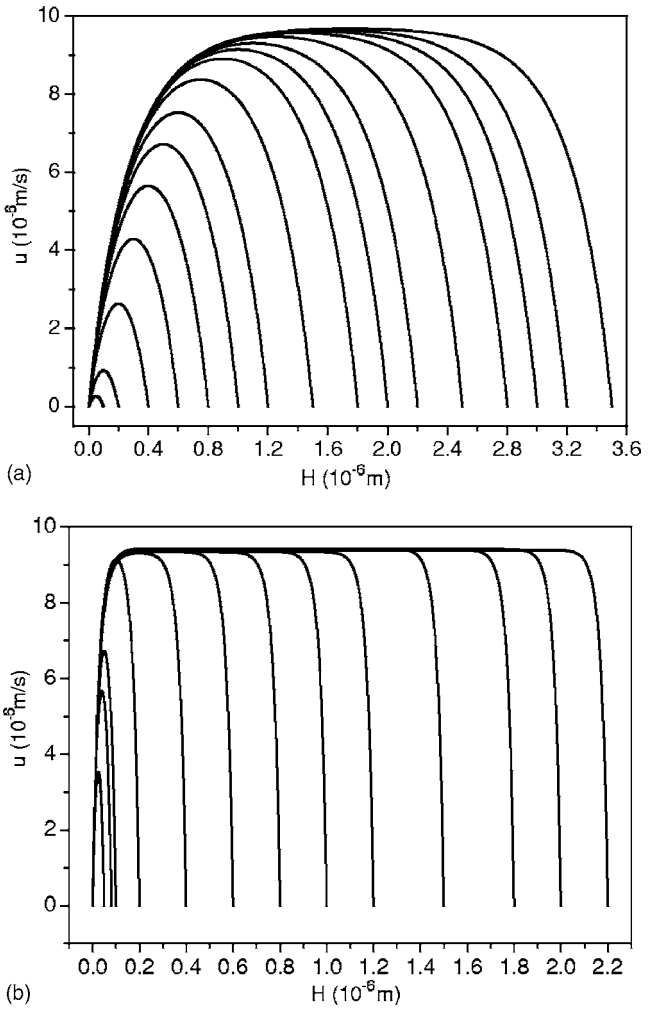

FIG. 6. The streamwise velocity profiles for various channel heights. (a) $c_\infty = 10^{-6}$ mol/l, the Debye length is 0.2915 μm, $\zeta = -50$ mV, and $E = 500$ V/m. From the left to the right, the channel heights are $H = 0.1$, 0.2, 0.4, 0.6, 0.8, 1.0, 1.2, 1.5, 1.8, 2.0, 2.2, 2.5, 2.8, 3.0, 3.2, and 3.5 μm, respectively. (b) $c_\infty = 10^{-4}$ mol/l, the Debye length is 0.029 15 μm, $\zeta = -50$ mV, and $E = 500$ V/m. From the left to the right, the channel heights are $H = 0.05$, 0.08, 0.1, 0.2, 0.4, 0.6, 0.8, 1.0, 1.2, 1.5, 1.8, 2.0, and 2.2 μm, respectively.

C. Electroosmotic flow in heterogeneous microchannels

Let us consider a channel consisting different materials. The employed nonuniform surface potentials are shown in Fig. 8 and Table I. It may be possible to fabricate such a microchannel by using different materials on various portions of the channel surface. In practice, it is also possible to obtain variations in the zeta potential due to the contamination in the microchannel walls, variations in the wall coating, or gradients in the buffer p_H.[2,4] The studied total streamwise length of the channel is six times of the channel height. In the simulations, we set $E = 500$ V/m, $c_\infty = 10^{-4}$ mol/l, and the corresponding Debye length is 0.029 15 μm.

In Fig. 9 case 3 can be regarded as a heterogeneous surface with symmetrically distributed patches, which implies that the zeta potentials on the upper and lower surfaces are exactly the same in terms of both magnitude and sign. Case 1 and case 2 can be regarded as asymmetric with the same magnitude but opposite sign. We can see that local

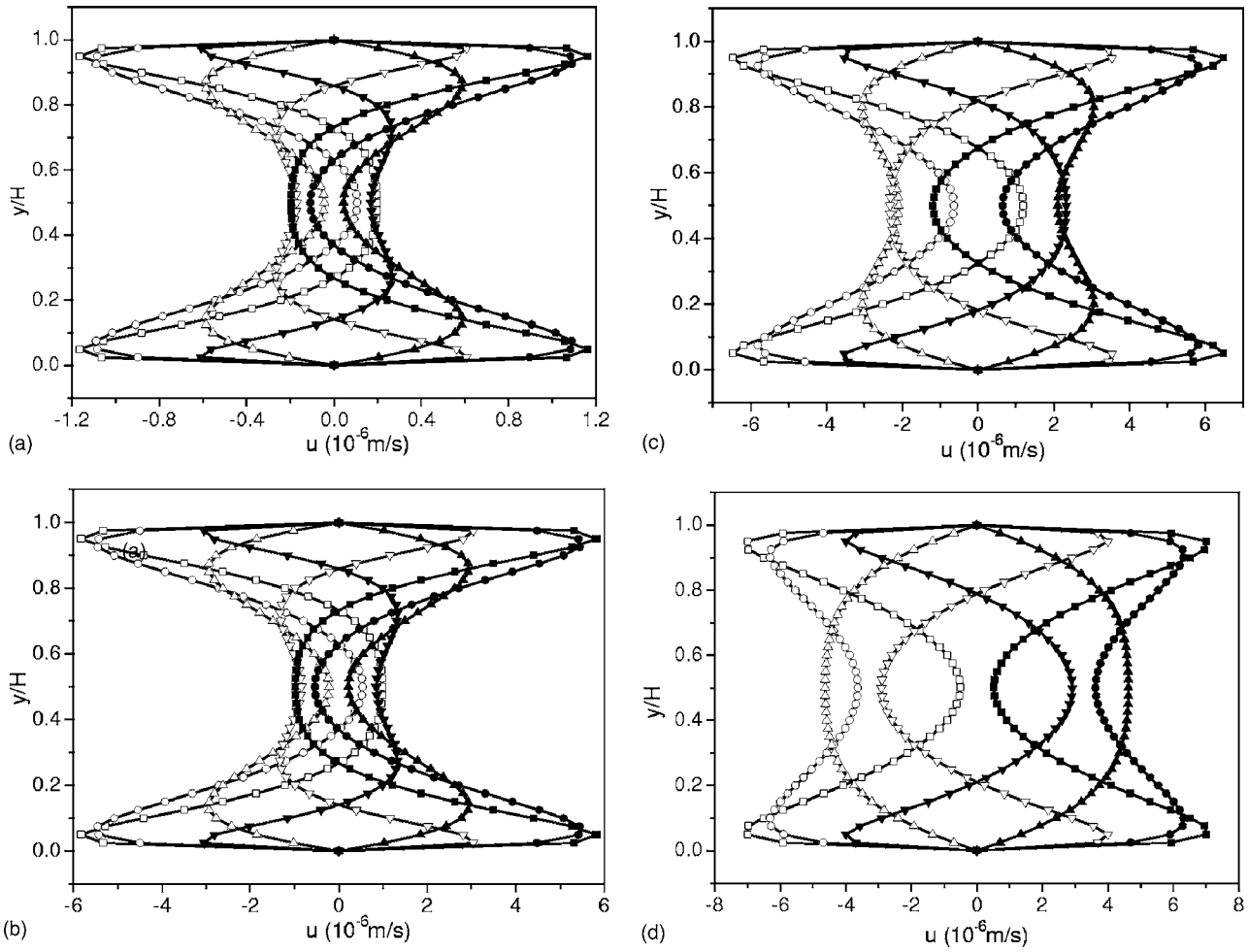

FIG. 7. The velocity distribution for time periodic electroosmotic flow at different times. The open squares, circles, triangles, and inverted triangles represent the results at $t=0$, $T_E/8$, $T_E/4$, $3T_E/8$, respectively; the closed squares, circles, triangles, and inverted triangles represent the results at $t=T_E/2$, $5T_E/8$, $3T_E/4$, and $7T_E/8$, respectively. (a) $E_0=100$ V/m, $T_E=20\,000$, and $\zeta=-50$ mV. (b) $E_0=500$ V/m, $T_E=20\,000$, and $\zeta=-50$ mV. (c) $E_0=500$ V/m, $T_E=40\,000$, and $\zeta=-50$ mV. (d) $E_0=500$ V/m, $T_E=80\,000$, and $\zeta=-50$ mV.

circulations can occur near a heterogeneous region. The fluid rotates in opposite directions in red (dark) and blue (white) areas and the sizes of the vortex appear to be the same. Also the absolute values of the maximum velocities in each vortex are the same. The different sizes of circulation regions between case 1 and case 2 show that the dimension of the heterogeneous patches has significant effect on the flow field patterns. For different distributions of the surface potential, the secondary flow in the channel varies much. Comparing case 3 with case 2 we can find that opposite vortices exist in the streamwise direction for case 2 while opposite vorteces exist both in the streamwise direction and spanwise direction simultaneously. The mixing effect for case 3 is obviously more enhanced. We can make the flow patterns transform periodically from case 1 to case 3 by controlling the wall zeta potential periodically. Thus we can increase the disturbance in the fluid and enhance the mixing efficiency remarkably.

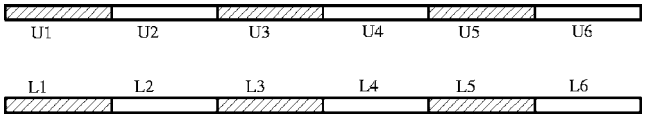

FIG. 8. Schematic of the surfaces with nonuniform surface potential.

D. Electroosmotic pulsating flow in heterogeneous microchannels

In this section, we investigated the electroosmotic pulsating flow in heterogeneous microchannels. The studied channel, the nonuniform wall potential distribution, and the bulk ionic molar concentration are the same with those in the above section. But the external electric field parallel to the channel length alternates with the time periodically as in Eq. (25) with $E_0=500$ V/m.

To save article space, we just show in Fig. 10 the streamlines for case 2 at eight different times. We can see that different flow patterns occur at different times. From the transformation between the eight different streamlines, we can see that the fluid can be mixed completely both in the streamwise direction and in the spanwise direction in one

TABLE I. Heterogeneous zeta potential distribution normalized by $\zeta_0=50$ mV on the upper and lower walls.

Case	U1/L1	U2/L2	U3/L3	U4/L4	U5/L5	U6/L6
1	1/−1	1/−1	−1/1	−1/1	1/−1	−1/−1
2	1/−1	−1/1	1/−1	−1/1	1/−1	1/−1
3	1/1	−1/−1	1/1	−1/−1	1/1	−1/−1

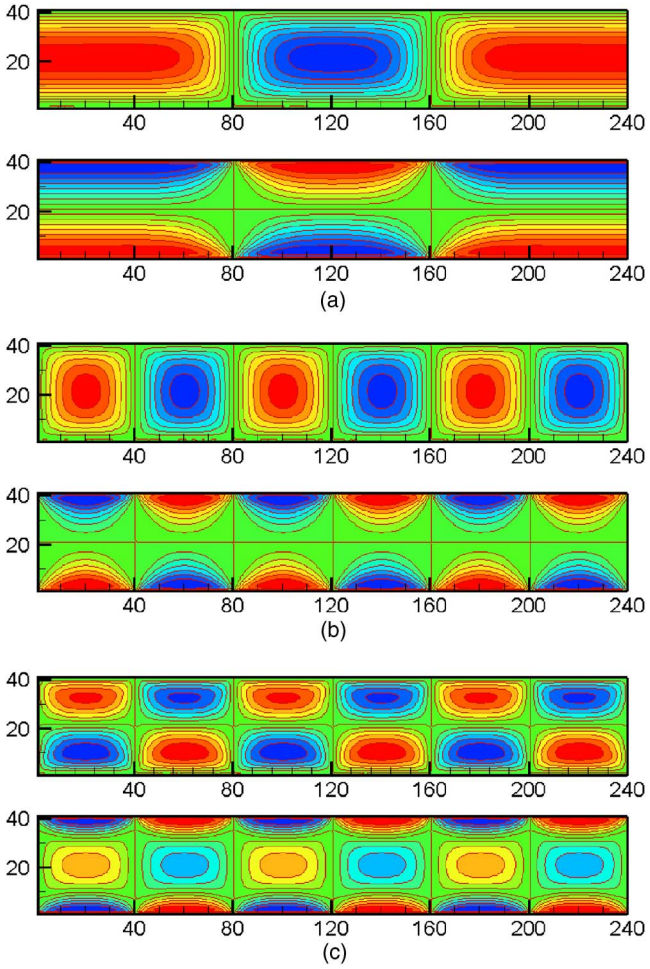

FIG. 9. (Color online) Streamlines (the upper) and isolines of the streamwise velocity (the bottom) for heterogeneous surface potential cases. (a) Case 1. (b) Case 2. (c) Case 3.

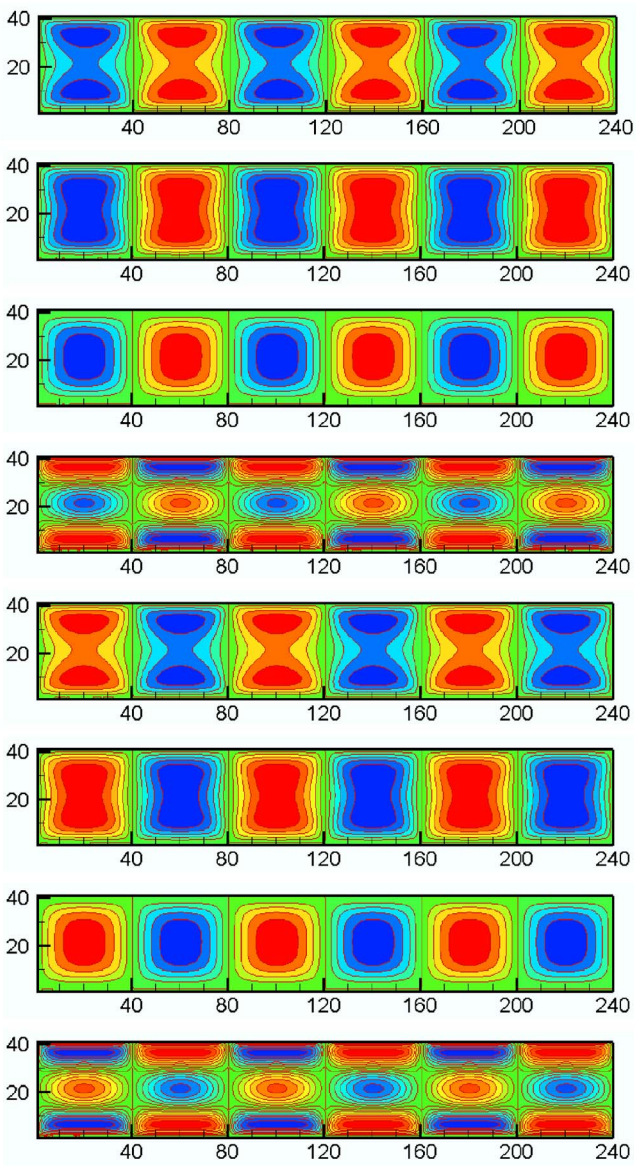

FIG. 10. (Color online) Streamlines at eight different times. From the upper to the bottom, $t=0$, $T_E/8$, $T_E/4$, $3T_E/8$, $T_E/2$, $5T_E/8$, $3T_E/4$, and $7T_E/8$.

period. This enables a reduction in the mixing channel length and an improved degree of mixing efficiency.

V. CONCLUSIONS

Motivated by the growing interest in electroosmosis as a reliable no moving parts strategy to pump liquid, to mix liquid, and to control fluid motion in microfluidic devices, we have studied steady-state and pulsating electroosmosis flow in two-dimensional parallel uniform and nonuniform charged microchannels. We have used a lattice Boltzmann equation, which recovers the nonlinear Poisson-Boltzmann equation, to solve the electric potential distribution in the electrolytes, and used another lattice Boltzmann equation, which recovers the Navier-Stokes equation including the external force term, to solve the velocity fields. We have validated the method using the electric potential distribution and the pressure driven pulsating flow which both have analytical solutions.

For the electroosmotic flow in homogeneous microchannels, by studying the effects of the bulk ionic concentration and channel height, we find that the velocity profiles exhibit a sharp variation very near the walls and the maximum velocity nearly keeps a constant in the most of the channel centerline regions if the ratio of the channel height to the Debye length is larger than about 10.

If the Debye length is much lower than the channel height, the velocity in the electroosmotic flow nearly increases proportionally as the zeta potential increases or as the external electric field intensity increases. However, if the Debye length is comparable to the channel height, the maximum velocity in the electroosmotic flow still nearly increases proportionally with the increase of the external electric field intensity while the maximum velocity increases more rapidly as the zeta potential increases.

For the electroosmotic pulsating flow in homogeneous microchannels, the magnitude of the velocity increases proportionally as the external electric field intensity increases. Annular effects are strong in the velocity profiles when the period is short. As the frequency decreases, the annular effect weakens in the channel.

For the electroosmotic flow and electroosmotic pulsating flow in heterogeneous microchannels, heterogeneous surface potential distribution can improve mixing efficiency greatly. For pulsating flow in heterogeneous microchannels, the fluid can be mixed completely in the whole microchannel in one period if the heterogeneous surface potentials are distributed correctly. This allows one to design microfluidic mixers with high efficiency that utilize chaotic advection without any moving components.

ACKNOWLEDGMENT

This work was supported by the National Natural Science Foundation of China (Grant Nos. 50406020 and 50425620).

[1]M. Gad-el-Hak, J. Fluids Eng. **121**, 5 (1999).
[2]P. Dutta, Ph. D. thesis, Texas A&M University, 2001.
[3]O. Soderman and B. Jonsson, J. Chem. Phys. **105**, 10300 (1996).
[4]N. G. Green, A. Ramos, A. Gonzalez, H. Morgan, and A. Castellanos, Phys. Rev. E **61**, 4011 (2000).
[5]A. Gonzalez, A. Ramos, N. G. Green, A. Castellanos, and H. Morgan, Phys. Rev. E **61**, 4019 (2000).
[6]V. M. Barragan and C. R. Bauza, J. Colloid Interface Sci. **230**, 359 (2000).
[7]M. Scott, K. V. I. S. Kaler, and R. Paul, J. Colloid Interface Sci. **238**, 449 (2001).
[8]M. H. Oddy, J. G. Santiago, and J. C. Mikkelsen, Anal. Chem. **73**, 5822 (2001).
[9]D. Lastochkin, R. H. Zhou, P. Wang, Y. X. Ben, and H. C. Chang, J. Appl. Phys. **96**, 1730 (2004).
[10]M. Campisi, D. Accoto, and P. Dario, J. Chem. Phys. **123**, 204724 (2005).
[11]C. A. Keely, T. A. A. M. van de Goor, and D. McManigil, Anal. Chem. **66**, 4236 (1994).
[12]A. Ajdari, Phys. Rev. Lett. **75**, 755 (1995).
[13]A. Ajdari, Phys. Rev. E **53**, 4996 (1996).
[14]A. D. Stroock, M. Weck, D. T. Chiu, W. T. S. Huck, P. J. A. Kenis, R. F. Ismagilov, and G. M. Whitesides, Phys. Rev. Lett. **84**, 3314 (2000).
[15]A. E. Herr, J. I. Molho, J. G. Santiago, M. G. Mungal, T. W. Kenny, and M. G. Garguilo, Anal. Chem. **72**, 1053 (2000).
[16]L. Q. Ren and D. Q. Li, J. Colloid Interface Sci. **243**, 255 (2001).
[17]D. Erickson and D. Q. Li, Langmuir **18**, 1883 (2002).
[18]S. Z. Qian and H. H. Bau, Anal. Chem. **74**, 3616 (2002).
[19]L. M. Fu, J. Y. Lin, and R. J. Yang, J. Colloid Interface Sci. **258**, 266 (2003).
[20]F. Z. Tian, B. M. Li, and D. Y. Kwok, Langmuir **21**, 1126 (2005).
[21]F. Z. Tian and D. Y. Kwok, Langmuir **21**, 2192 (2005).
[22]S. C. Jacobson, T. E. McKnight, and J. M. Ramsey, Anal. Chem. **71**, 4455 (1999).
[23]C. C. Chang and R. J. Yang, J. Micromech. Microeng. **14**, 550 (2004).
[24]R. H. Liu, M. A. Stremler, K. V. Sharp, M. G. Olsen, J. G. Santiago, R. J. Adrian, H. Aref, and D. J. Beebe, J. Microelectromech. Syst. **9**, 190 (2000).
[25]A. D. Stroock, S. K. Dertinger, A. Ajdari, I. Mezic, H. A. Stone, and G. M. Whitesides, Science **295**, 647 (2002).
[26]A. D. Stroock, S. K. Dertinger, G. M. Whitesides, and A. Ajdari, Anal. Chem. **74**, 5306 (2002).
[27]S. Chen and G. D. Doolen, Annu. Rev. Fluid Mech. **30**, 329 (1998).
[28]X. B. Nie, G. D. Doolen, and S. Y. Chen, J. Stat. Phys. **107**, 279 (2002).
[29]C. Y. Lim, C. Shu, X. D. Niu, and Y. T. Chew, Phys. Fluids **14**, 2299 (2002).
[30]G. H. Tang, W. Q. Tao, and Y. L. He, Int. J. Mod. Phys. C **15**, 335 (2004).
[31]G. H. Tang, W. Q. Tao, and Y. L. He, Phys. Fluids **17**, 058101 (2005).
[32]Y. H. Zhang, R. S. Qin, and D. R. Emerson, Phys. Rev. E **71**, 047702 (2005).
[33]G. H. Tang, W. Q. Tao, and Y. L. He, J. Appl. Phys. **97**, 104918 (2005).
[34]G. H. Tang, W. Q. Tao, and Y. L. He, Phys. Rev. E **72**, 056301 (2005).
[35]J. Horbach and D. Frenkel, Phys. Rev. E **64**, 061507 (2001).
[36]S. Melchionna and S. Succi, J. Chem. Phys. **120**, 4492 (2004).
[37]F. Capuani, I. Pagonabarraga, and D. Frenkel, J. Chem. Phys. **121**, 973 (2004).
[38]B. M. Li and D. Y. Kwok, Langmuir **19**, 3041 (2003).
[39]Z. L. Guo, T. S. Zhao, and Y. Shi, J. Chem. Phys. **122**, 144907 (2005).
[40]X. Y. He and L. S. Luo, Phys. Rev. E **56**, 6811 (1997).
[41]P. L. Bhatnagar, E. P. Gross, and M. Krook, Phys. Rev. **94**, 511 (1954).
[42]Y. H. Qian, D. d'Humieres, and P. Lallemand, Europhys. Lett. **17**, 479 (1992).
[43]X. Y. He, S. Chen, and G. D. Doolen, J. Comput. Phys. **146**, 282 (1998).
[44]D. W. Grunau, Ph.D. thesis, Colorado State University, 1993.
[45]J. Santiago, Anal. Chem. **73**, 2353 (2001).
[46]C. L. Rice and R. Whitehead, J. Phys. Chem. **69**, 4017 (1965).
[47]C. Yang and D. Q. Li, Colloids Surf., A **14**, 339 (1998).
[48]R. J. Flatt and P. Bowen, Cem. Concr. Res. **33**, 781 (2003).
[49]X. Y. He, Q. Zou, L. S. Luo, and M. Dembo, J. Stat. Phys. **87**, 115 (1997).
[50]D. P. Ziegler, J. Stat. Phys. **71**, 1171 (1993).
[51]T. Inamuro, M. Yoshino, and F. Ogino, Phys. Fluids **7**, 2928 (1995).
[52]Q. Zou and X. Y. He, Phys. Fluids **9**, 1591 (1997).
[53]S. Chen, D. Martinez, and R. W. Mei, Phys. Fluids **8**, 2527 (1996).
[54]A. D' Orazio, S. Succi, and C. Arrighetti, Phys. Fluids **15**, 2778 (2003).
[55]G. H. Tang, W. Q. Tao, and Y. L. He, Phys. Rev. E **72**, 016703 (2005).
[56]I. G. Currie, *Fundamental Mechanics of Fluids* (McGraw-Hill, New York, 1997).